CHEMISTRY OF MATERIALS
Article

Chem. Mater. **2009,** *21,* 2803–2809 2803
DOI:10.1021/cm900709w

Nanosized Carbon Particles From Natural Gas Soot

Lei Tian,[†,‡] Debraj Ghosh,[‡] Wei Chen,[‡] Sulolit Pradhan,[‡] Xijun Chang,[†] and Shaowei Chen*[,‡]

[†]*Department of Chemistry, Lanzhou University, Lanzhou, Gansu 730000, P.R. China, and* [‡]*Department of Chemistry and Biochemistry, University of California, 1156 High Street, Santa Cruz, California 95064*

Received March 12, 2009. Revised Manuscript Received April 24, 2009

Carbon nanoparticles were prepared by refluxing the combustion soot of natural gas in nitric acid. Transmission Electron Microscopy measurements showed that the resulting particles exhibited an average diameter of 4.8 ± 0.6 nm, and the crystalline lattices were consistent with graphitic carbons. ^{13}C NMR and FTIR spectroscopic measurements further confirmed the presence of sp^2 carbons in the form of aryl and carboxylic/carbonyl moieties. The resulting carbon nanoparticles were found to emit photoluminescence with a quantum yield of approximately 0.43%. Additionally, the emission band energy of the carbon nanoparticle was very similar to that of much smaller carbon nanoparticles obtained from candle soot, suggesting that the photoluminescence might arise from particle surface states, analogous to the behaviors of semiconductor quantum dots with an indirect bandgap. In electrochemical measurements, two pairs of well-defined voltammetric waves were observed, which might be ascribed to the peripheral functional moieties that were analogous to phenanthrenequinone derivatives. Interestingly, the carbon nanoparticles might also be exploited as nanoscale structural scaffolds for the deposition of nanostructures of varied transition metals, leading to the formation of metal−carbon functional nanocomposites.

Introduction

Carbon is one of the most abundant elements in nature. A wide variety of carbon-based nanomaterials have been prepared, such as carbon nanotubes, fullerenes, nanofibers, nanodiamond, carbon nanoonions, and other carbonaceous nanomaterials. The immense research interest is primarily driven by their potential applications as a high performance material in a broad range of areas. For example, in environmental research, carbon nanomaterials have been used as sorbents,[1−6] high-flux membranes,[7,8] depth filters,[9−11] antimicrobial agents,[12−14] environmental sensors,[15−17] renewable energy technologies,[18−20] and pollution prevention materials.[21] In biological science, carbon-based tubular nanostructures have been utilized as excellent platforms for facilitating biochemical reactions and processes, such as sensitive recognition of antibodies,[22] sequencing of nucleic acids,[23] bioseparation and biocatalysis,[24] and ion channel blocking.[25] Fullerenes have also been employed as neuroprotective agents,[26] HIV-1 protease inhibitors,[27] X-ray contrast enhancers,[28]

*To whom correspondence should be addressed. E-mail: schen@chemistry.ucsc.edu.

(1) Pignatello, J. J.; Xing, B. S. *Environ. Sci. Technol.* **1996**, *30*, 1–11.
(2) Allen-King, R. M.; Grathwohl, P.; Ball, W. P. *Adv. Water Resour.* **2002**, *25*, 985–1016.
(3) Bailey, S. E.; Olin, T. J.; Bricka, R. M.; Adrian, D. D. *Water Resour.* **1999**, *33*, 2469–2479.
(4) Luthy, R. G.; Aiken, G. R.; Brusseau, M. L.; Cunningham, S. D.; Gschwend, P. M.; Pignatello, J. J.; Reinhard, M.; Traina, S. J.; Weber, W. J.; Westall, J. C. *Environ. Sci. Technol.* **1997**, *31*, 3341–3347.
(5) Weber, W. J.; Mcginley, P. M.; Katz, L. E. *Water Resour.* **1991**, *25*, 499–528.
(6) Schwarzenbach, R. P.; Westall, J. *Environ. Sci. Technol.* **1981**, *15*, 1360–1367.
(7) Shannon, M. A.; Bohn, P. W.; Elimelech, M.; Georgiadis, J. G.; Marinas, B. J.; Mayes, A. M. *Nature* **2008**, *452*, 301–310.
(8) Jirage, K. B.; Hulteen, J. C.; Martin, C. R. *Science* **1997**, *278*, 655–658.
(9) Cong, H. L.; Zhang, J. M.; Radosz, M.; Shen, Y. Q. *J. Membr. Sci.* **2007**, *294*, 178–185.
(10) Peng, F. B.; Hu, C. L.; Jiang, Z. Y. *J. Membr. Sci.* **2007**, *297*, 236–242.
(11) Choi, J. H.; Jegal, J.; Kim, W. N. *J. Membr. Sci.* **2006**, *284*, 406–415.
(12) Colvin, V. L. *Nat. Biotechnol.* **2003**, *21*, 1166–1170.
(13) Nel, A.; Xia, T.; Madler, L.; Li, N. *Science* **2006**, *311*, 622–627.
(14) Lam, C. W.; James, J. T.; McCluskey, R.; Arepalli, S.; Hunter, R. L. *Crit. Rev. Toxicol.* **2006**, *36*, 189–217.
(15) Valentini, F.; Biagiotti, V.; Lete, C.; Palleschi, G.; Wang, J. *Sens. Actuators, B* **2007**, *128*, 326–333.
(16) Kim, S. N.; Rusling, J. F.; Papadimitrakopoulos, F. *Adv. Mater.* **2007**, *19*, 3214–3228.
(17) Allen, B. L.; Kichambare, P. D.; Star, A. *Adv. Mater.* **2007**, *19*, 1439–1451.
(18) Carrette, L.; Friedrich, K. A.; Stimming, U. *ChemPhysChem* **2000**, *1*, 162–193.
(19) Kamat, P. V.; Haria, M.; Hotchandani, S. *J. Phys. Chem. B* **2004**, *108*, 5166–5170.
(20) Kamat, P. V. *J. Phys. Chem. C* **2007**, *111*, 2834–2860.
(21) Mauter, M. S.; Elimelech, M. *Environ. Sci. Technol.* **2008**, *42*, 5843–5859.
(22) Chen, R. J.; Bangsaruntip, S.; Drouvalakis, K. A.; Kam, N. W. S.; Shim, M.; Li, Y. M.; Kim, W.; Utz, P. J.; Dai, H. J. *Proc. Nat. Acad. Sci. U.S.A.* **2003**, *100*, 4984–4989.
(23) Wang, H. B.; Thoss, M. *J. Chem. Phys.* **2003**, *119*, 1289–1299.
(24) Mitchell, D. T.; Lee, S. B.; Trofin, L.; Li, N. C.; Nevanen, T. K.; Soderlund, H.; Martin, C. R. *J. Am. Chem. Soc.* **2002**, *124*, 11864–11865.
(25) Park, K. H.; Chhowalla, M.; Iqbal, Z.; Sesti, F. *J. Biol. Chem.* **2003**, *278*, 50212–50216.
(26) Dugan, L. L.; Turetsky, D. M.; Du, C.; Lobner, D.; Wheeler, M.; Almli, C. R.; Shen, C. K. F.; Luh, T. Y.; Choi, D. W.; Lin, T. S. *Proc. Nat. Acad. Sci. U.S.A.* **1997**, *94*, 9434–9439.
(27) Sijbesma, R.; Srdanov, G.; Wudl, F.; Castoro, J. A.; Wilkins, C.; Friedman, S. H.; Decamp, D. L.; Kenyon, G. L. *J. Am. Chem. Soc.* **1993**, *115*, 6510–6512.
(28) Wharton, T.; Wilson, L. J. *Tetrahedron Lett.* **2002**, *43*, 561–564.

Published on Web 05/15/2009

and drug delivery transporters.[29] More recently, nitrogen-doped carbon nanotube arrays have been found to exhibit marked enhancement of electrocatalytic activity, long-term operation, stability, and tolerance to crossover effects in comparison to platinum for oxygen reduction reactions in alkaline fuel cells.[30] The unique chemical and physical properties of carbon nanomaterials are largely attributed to their high surface area, special morphology, unique electronic, optical, and thermal characteristics, biocompatibility, and chemical inertness.[31−43]

Among these various forms of carbon nanomaterials, carbon nanoparticles represent a unique class of functional materials that warrant further and more thorough investigation. Typically, these nanoparticles are prepared by laser ablation. For instance, Hu et al.[38] synthesized photoluminescent carbon nanoparticles of 3 nm in diameter by laser irradiation of a suspension of carbon powders in an organic solvent. Sun and co-workers[44] demonstrated that carbon nanoparticles might be produced by laser ablation of a carbon target in the presence of water vapor with argon as the carrier gas, and subsequent surface passivation with simple organic ligands rendered the particles to emit strong photoluminescence. Carbon nanoparticles have also been prepared by electrochemical treatments of multiwall carbon nanotubes, as demonstrated by Zhou and co-workers[45] where carbon nanoparticles of spherical shape and narrow size distribution (2.8 ± 0.5 nm in diameter) were formed.

More recently, a very simple and yet effective synthetic protocol[46] was reported for the preparation of multicolor luminescent carbon nanoparticles (~1 nm in diameter) from the combustion soot of candles. In the present study, the procedure was adopted to synthesize carbon nanoparticles from the combustion soot of natural gas (instead of candles). After thermal refluxing in acid, the obtained carbon nanoparticles become water-soluble and may be readily purified by dialysis. Despite the large particle size (ca. 5 nm in diameter), the particles exhibit similar photoluminescence characteristics as compared to those from candle soot, suggesting that the nanoparticles behave as indirect bandgap materials and the surface trap states are responsible for the photoluminescence properties. Interestingly, these carbon nanomaterials may also be used as a unique structural scaffold on which nanostructures of varied transition metals may be deposited, leading to the formation of functional nanocomposite materials.

Experimental Section

Chemicals. Nitric acid (HNO_3, 69.8%, Fisher), sodium carbonate (Na_2CO_3, 99+%, Aldrich), silver nitrate ($AgNO_3$, Matheson Coleman & Bell), palladium chloride ($PdCl_2$, MP Biomedicals), cupric nitrate ($Cu(NO_3)_2$, Matheson Coleman & Bell, 99.5%), sodium chloride (NaCl), and ascorbic acid (99%, ACROS) were all used as received. Water was supplied by a Barnstead Nanopure Water System (18.3 MΩ·cm).

Synthesis of Carbon Nanoparticles. Carbon nanoparticles were prepared by adopting a procedure reported in the literature.[46] Briefly, carbon soot was collected on the inside wall of a glass beaker by placing the beaker upside-down above the flame of a natural gas burner. Typically 100 mg of the soot was then refluxed in 10 mL of 5 M HNO_3 for 12 h. When cooled downed to room temperature, the brownish yellow supernatant after centrifugation was neutralized by Na_2CO_3, and then dialyzed against Nanopure water through a dialysis membrane for 3 days, affording purified carbon nanoparticles.

Deposition of Metal Nanostructures on Carbon Nanoparticles. In a typical reaction, 5 mg of carbon nanoparticles was dissolved in 5 mL of water. Then a water solution of selected metal salts ($AgNO_3$, $Cu(NO_3)_2$, or $PdCl_2$) at a concentration of 1 mg/mL was added into the carbon particle solution under magnetic stirring. The mixture was allowed to stir overnight, to which a calculated amount of ascorbic acid was added in a dropwise fashion. The solution color changed gradually from light brown to dark red for silver, to dark yellow for copper, and to black for palladium. The observed coloration signified the formation of metal nanostructures. Excessive salts were then removed by dialysis against Nanopure water, and the metal/carbon nanocomposite materials remained soluble in water.

Transmission Electron Microscopy (TEM). The particle core diameter and lattice fringes were examined with a JEOL 2100-F 200 KV Field-Emission Analytical Transmission Electron Microscope in the Molecular Foundry and the National Center for Electron Microscopy at Lawrence Berkeley National Laboratory. The samples were prepared by casting a drop of the particle solution (~1 mg/mL) in Nanopure water onto a 200-mesh holey carbon-coated copper grid. The particle diameter was estimated by using ImageJ software analysis of the TEM micrographs. Elemental analysis of the carbon−metal nanostructures was also carried out by high solid-angle energy-dispersive X-ray analysis with a Gatan Tridiem spectrometer used for energy-filtered imaging.

(29) Ashcroft, J. M.; Tsyboulski, D. A.; Hartman, K. B.; Zakharian, T. Y.; Marks, J. W.; Weisman, R. B.; Rosenblum, M. G.; Wilson, L. J. *Chem. Commun*. **2006**, 3004–3006.
(30) Gong, K. P.; Du, F.; Xia, Z. H.; Durstock, M.; Dai, L. M. *Science* **2009**, *323*, 760–764.
(31) Avouris, P. *Chem. Phys*. **2002**, *281*, 429–445.
(32) Ebbesen, T. W.; Tanigaki, K.; Kuroshima, S. *Chem. Phys. Lett*. **1991**, *181*, 501–504.
(33) Zhu, S. B.; Xu, T. G.; Fu, H. B.; Zhao, J. C.; Zhu, Y. F. *Environ. Sci. Technol*. **2007**, *41*, 6234–6239.
(34) Saito, Y.; Uemura, S. *Carbon* **2000**, *38*, 169–182.
(35) Hamada, N.; Sawada, S.; Oshiyama, A. *Phys. Rev. Lett*. **1992**, *68*, 1579–1581.
(36) Tans, S. J.; Devoret, M. H.; Dai, H. J.; Thess, A.; Smalley, R. E.; Geerligs, L. J.; Dekker, C. *Nature* **1997**, *386*, 474–477.
(37) Yu, S. J.; Kang, M. W.; Chang, H. C.; Chen, K. M.; Yu, Y. C. *J. Am. Chem. Soc*. **2005**, *127*, 17604–17605.
(38) Hu, S. L.; Niu, K. Y.; Sun, J.; Yang, J.; Zhao, N. Q.; Du, X. W. *J. Mater. Chem*. **2009**, *19*, 484–488.
(39) Kong, X. L.; Huang, L. C. L.; Hsu, C. M.; Chen, W. H.; Han, C. C.; Chang, H. C. *Anal. Chem*. **2005**, *77*, 259–265.
(40) Ushizawa, K.; Sato, Y.; Mitsumori, T.; Machinami, T.; Ueda, T.; Ando, T. *Chem. Phys. Lett*. **2002**, *351*, 105–108.
(41) Cao, L.; Wang, X.; Meziani, M. J.; Lu, F. S.; Wang, H. F.; Luo, P. J. G.; Lin, Y.; Harruff, B. A.; Veca, L. M.; Murray, D.; Xie, S. Y.; Sun, Y. P. *J. Am. Chem. Soc*. **2007**, *129*, 11318.
(42) Kong, X. L.; Huang, L. C. L.; Liau, S. C. V.; Han, C. C.; Chang, H. C. *Anal. Chem*. **2005**, *77*, 4273–4277.
(43) Glinka, Y. D.; Lin, K. W.; Chang, H. C.; Lin, S. H. *J. Phys. Chem. B* **1999**, *103*, 4251–4263.
(44) Sun, Y. P.; Zhou, B.; Lin, Y.; Wang, W.; Fernando, K. A. S.; Pathak, P.; Meziani, M. J.; Harruff, B. A.; Wang, X.; Wang, H. F.; Luo, P. J. G.; Yang, H.; Kose, M. E.; Chen, B. L.; Veca, L. M.; Xie, S. Y. *J. Am. Chem. Soc*. **2006**, *128*, 7756–7757.
(45) Zhou, J. G.; Booker, C.; Li, R. Y.; Zhou, X. T.; Sham, T. K.; Sun, X. L.; Ding, Z. F. *J. Am. Chem. Soc*. **2007**, *129*, 744–745.
(46) Liu, H. P.; Ye, T.; Mao, C. D. *Angew. Chem., Int. Ed*. **2007**, *46*, 6473–6475.

Spectroscopies. UV−vis spectroscopic studies were performed with an ATI Unicam UV4 spectrometer by using a 1 cm quartz cuvette with a resolution of 2 nm. Photoluminescence measurements were carried out with a PTI photoluminescence spectrometer. ^{13}C NMR spectra were collected with a Varian Oxford 600 MHz spectrometer by dissolving 50 mg of carbon nanoparticles in 700 μL of deuterized water. Infrared spectra were acquired with a Perkin-Elmer Precision Spectrum One FTIR spectrometer.

Electrochemistry. Cyclic voltammetric measurements were carried out with a CHI 440 electrochemical workstation. A glassy carbon electrode (diameter 3 mm, from Bioanalytical Systems, Inc.) was used as the working electrode. A Ag/AgCl wire and a Pt coil were used as the reference and counter electrode, respectively. The electrolyte solutions were deaerated with ultrahigh-purity N_2 for 10 min before the acquisition of electrochemical data, and the electrolyte solution was blanketed with a nitrogen atmosphere during the entire experimental procedure.

Results and Discussions

Carbon Nanoparticles. The formation of carbon nanoparticles was first confirmed by TEM measurements. TEM has been used extensively as a powerful tool in the study of nanoscale materials, from which the size, morphology, and crystalline lattices may be identified. Figure 1A shows a representative TEM micrograph of the carbon nanoparticles. It can be seen that the particles are mostly of spherical shape and dispersed rather evenly on the TEM grid surface. The size dispersity of the particles can be seen to be relatively small, with the majority of the particles falling within the range of 4.4 to 5.4 nm in diameter, as depicted in the size histogram in the figure inset. In fact, based on statistical analysis of several hundred particles the average diameter of the carbon nanoparticles was found to be 4.8 ± 0.6 nm. The crystalline nature of the carbon particles was then examined by high-resolution TEM measurements. A representative HRTEM micrograph is shown in panel B. In addition to what appears to be amorphous carbon materials, various lattice planes can be clearly identified with a spacing of 0.208 nm (identified by white arrows). Whereas this may be attributable both to the (103) diffraction plane of diamond-like (sp^3) carbon (analogous to SiC and ZnS, in reference to JCPDS cards 26-1081 and 26-1083) and to the (102) lattice of graphitic (sp^2) carbon (JCPDS 26-1076), further examinations suggest that the carbon nanoparticles obtained herein are of graphitic structure, as several other lattice fringes were also found with the lattice spacings of 0.334 nm, 0.194 nm, and 0.186 nm (Supporting Information, Figure S1), which are consistent with the (006), (104), and (105) diffraction planes of graphitic carbons (JCPDS 26-1076). These structural assignments are further supported by ^{13}C NMR measurements (vide infra). In the previous study carried out by Mao and co-workers,[46] the carbon nanoparticles obtained from candle soot were much smaller with the diameter around 1 nm, and because of this the crystalline structure of the particles was not identified. In a more recent study, Hu et al.[38] employed laser irradiation of carbon powders to prepare carbon nanoparticles. They also observed a lattice fringe of 0.20 nm in HRTEM

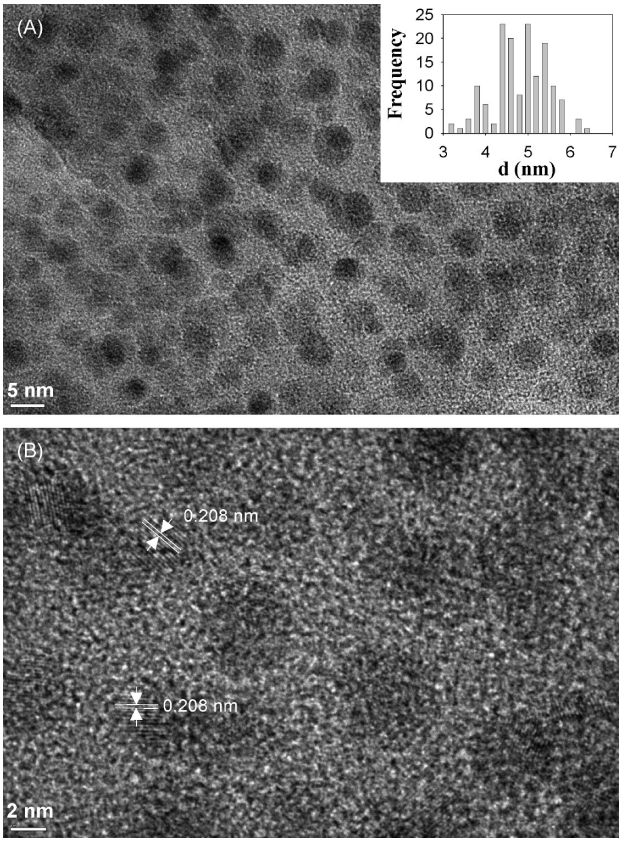

Figure 1. Representative TEM micrographs of carbon nanoparticles at (A) low and (B) high resolution. The scale bar is 5 nm in A and 2 nm in B. Inset to panel A depicts the particle size histogram. The crystalline lattices are identified in panel B.

measurements. On the basis of selected area electron diffractions, they proposed a diamond-like structure of the resulting carbon nanoparticles. It has to be noted that some of the lattice fringes of the diffraction planes of diamond-like and graphitic carbons are very close to each other, rendering it difficult to have an unambiguous assignment based on this experimental measurement alone. This is further complicated with nanosized carbon materials where the breakdown of symmetry at the nanoscale may cause a drastic difference in diffraction patterns in comparison to that of the bulk forms.

^{13}C NMR spectroscopy is a powerful technique in distinguishing sp^3 carbons from the sp^2 ones. Thus, it is exploited here to gain further structural insights about the carbon nanoparticles. As mentioned earlier, after thermal refluxing in concentrated HNO_3, the soot was broken up into particulate materials that became soluble in water. This is most likely because of the oxidative formation of peripheral carbonyl/carboxylic acid moieties, similar to the oxidative processing of carbon nanotubes by strong acids.[47] Such structural details may be revealed by ^{13}C NMR measurements, as aliphatic (sp^3) and aromatic (sp^2) carbons resonate differently, with the former in the range of 8 to 80 ppm whereas the latter in 90 to 180 ppm.[48] Figure 2 depicts

(47) Chen, J.; Hamon, M. A.; Hu, H.; Chen, Y. S.; Rao, A. M.; Eklund, P. C.; Haddon, R. C. *Science* **1998**, *282*, 95–98.
(48) MacKenzie, K. J. D.; Smith, M. E. Multinuclear solid-state NMR of inorganic materials, 1st ed.; Pergamon: Oxford, 2002.

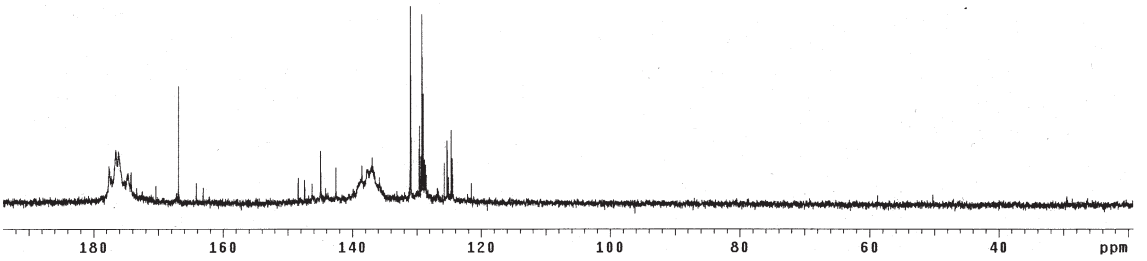

Figure 2. ^{13}C NMR spectrum of carbon nanoparticles in D_2O.

a ^{13}C NMR spectrum of the carbon particles prepared above (in D_2O). There are three features that warrant attention. First, below 120 ppm only a featureless profile can be seen, indicative of the absence of aliphatic (sp^3) carbons within the carbon nanoparticles (likewise, the presence of sp^1 carbons can also be excluded). That is, it is unlikely that the carbon nanoparticles are of diamond-like structure. Second, a series of peaks emerge within the range of 120 to 150 ppm, where the broad peak centered at 138 ppm may be ascribed to internal C=C sp^2 carbons and the peaks between 120 and 130 ppm are most likely to arise from (polycyclic) aromatic carbons, analogous to those of chrysene, pyrene, and so forth; and third, the peak between 170 and 180 ppm most probably arises from carboxylic/carbonyl carbons.[49] Note that in the previous study with carbon nanoparticles obtained from candle soot,[46] a peak at 114 ppm was also observed and attributed to terminal C=C bonds. This is not observed in the present study, implying that the terminal C=C bonds have most likely been oxidized into carboxylic/carbonyl moieties.

The presence of aromatic and carboxylic/carbonyl carbons is further supported in FTIR measurements, as manifested in Figure 3 (top curve). First, the broad peak centered at 3385 cm^{-1} may be attributed to the O−H vibrational stretch of the carboxylic moiety (and residual water), the shoulder at 1695 cm^{-1} to C=O vibration, and the peak at 1384 cm^{-1} to the symmetric carboxylate stretch.[50] In addition, a peak at 1600 cm^{-1} can be found which most likely arises from the C=C stretch of the aromatic rings, whereas the minor peak at 1045 cm^{-1} may be ascribed to the bending stretch of the carboxylic acid moieties.

On the basis of these measurements, the carbon nanoparticles obtained above most probably consist of a nanocrystalline core that features graphitic sp^2 carbons and is functionalized with carboxylic/carbonyl moieties on the particle surface (XPS measurements only showed the presence of two elements, C and O, Supporting Information, Figure S2). Interestingly, these nanoparticles exhibit unique photoluminescence properties. Figure 4 (black curves) shows the excitation and emission spectra of the carbon nanoparticles in water. A very well-defined excitation peak can be seen at 310 nm, and an emission peak at 420 nm, where the large energy discrepancy suggests that the particles behave as an indirect bandgap semiconductor material (UV−visible absorption measurements exhibit a largely featureless profile that is also consistent with indirect-bandgap semiconductor nanoparticles, Supporting Information, Figure S3). Certainly, further investigation is needed to confirm this hypothesis. Nonetheless, using rhodamine 6G as the comparative reference,[51] the quantum yield of the carbon nanoparticle photoluminescence was estimated to be 0.43%.

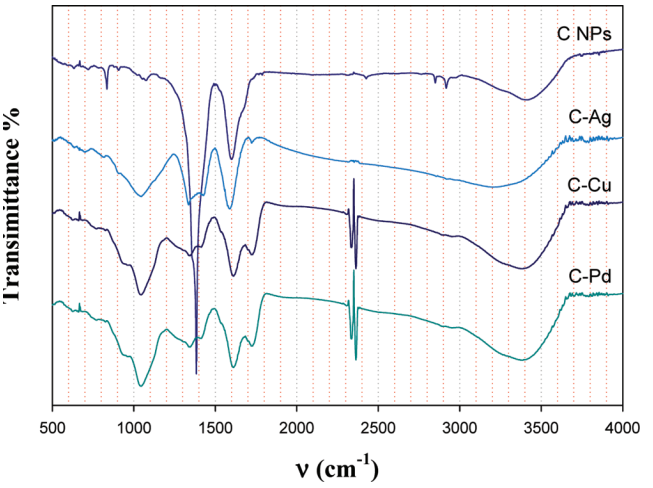

Figure 3. FTIR spectra of carbon nanoparticles before (C NPs) and after modification with various metal nanostructures (C−Ag, C−Cu, and C−Pd).

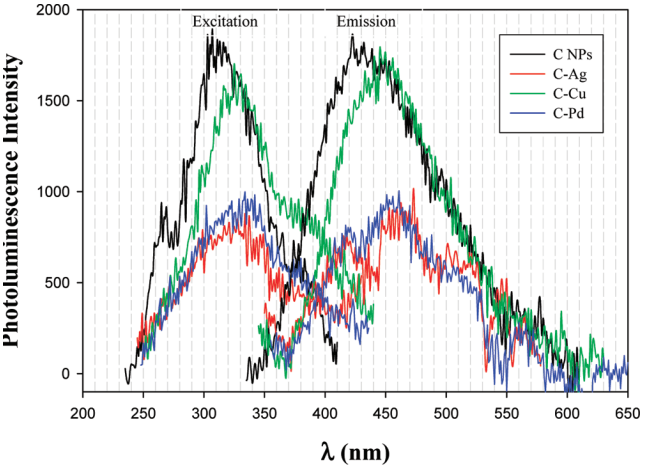

Figure 4. Excitation and emission spectra of carbon nanoparticles before (C NPs) and after modification with various metal nanostructures (C−Ag, C−Cu, and C−Pd) in water. Particle concentration 1 mg/mL.

(49) Details in the database, http://riodb01.ibase.aist.go.jp/sdbs/cgi-bin/cre_index.cgi?lang=eng.
(50) Silverstein, R. M.; Bassler, G. C.; Morrill, T. C. Spectrometric identification of organic compounds, 5th ed.; Wiley: New York, 1991.
(51) Kubin, R. F.; Fletcher, A. N. *J. Lumin.* **1982**, *27*, 455–462.

It is unlikely that these photoluminescence behaviors arose from simple aromatic complexes because the samples have been subjected to thermal refluxing in concentrated HNO_3 and extensive dialysis. The narrow emission band (full-width at half-maximum $\sim$ 120 nm) suggests a relatively small size dispersity of the particle, even without any fractionation treatment. This is consistent with the TEM results (Figure 1). It is also interesting to note that these photoluminescence properties are very similar to those observed with carbon nanoparticles obtained from candle soot,[46] despite the rather drastic difference in particle dimensions. One possible interpretation is that the photoluminescence arises from electronic transitions involving surface states of the particles, a rather common phenomenon with semiconductor quantum dots that exhibit an indirect bandgap[52] (mechanistically, the observed photoluminescence may be ascribed to the electronic transitions involving phenanthrenequinone moieties that are embedded within a conjugated aromatic matrix,[53] as suggested below by the electrochemical activity). In fact, this may also account for the effect of solution pH on the emission peak energy that was observed previously.[46]

Interestingly, the carbon nanoparticles obtained above also exhibited electrochemical activities. Figure 5 depicts the cyclic voltammograms of carbon nanoparticles in a water solution of 0.1 M KCl (pH $\sim$5) within the potential range of -1.0 V to $+1.0$ V at varied potential sweep rates. In comparison to the control experiment with a blank electrolyte solution (dashed curve), two pairs of voltammetric peaks can be seen with the formal potential at -0.28 V (peak I) and -0.06 V (peak II), respectively. Note that the peak splitting (ΔE_P) of peak I (250 mV at 0.1 V/s) is substantially larger than that of peak II (90 mV at 0.1 V/s), suggesting that the electron-transfer kinetics for peak I is markedly more sluggish than that of peak II. Additionally, with decreasing potential sweep rate (e.g., $\leq$0.04 V/s), the anodic waves of these two electron-transfer processes merge whereas the cathodic waves remain well separated and defined, implying the dynamic nature of the oxidative product in process I.

Additionally, the two electron-transfer reactions exhibit drastically different pH dependence, as depicted in the figure inset. It can be seen that within the pH range of 2 to 13, the formal potential of peak I remains virtually independent of pH, whereas that of peak II shows a cathodic shift of about 37 mV with the increase of one pH unit, suggesting the participation of protons in process II but not in process I.

The nature of these voltammetric behaviors remains unclear at this point. Yet it is unlikely that the observed voltammetric features arise from the electron-transfer reactions of carboxylic acid moieties on the nanoparticle surface, as the redox reactions of aromatic carboxylic acids typically occur at far more extreme electrode

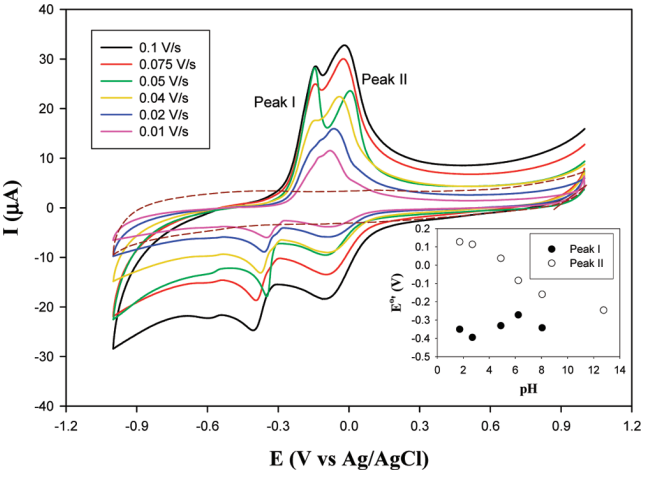

Figure 5. Cyclic voltammograms of a glassy carbon electrode (3 mm in dia.) in a water solution containing 0.1 M KCl and 1.5 mg/mL carbon nanopaticles (solid curves) at varied potential sweep rates (depicted as figure legends). The voltammogram of the same electrode in a 0.1 M KCl water solution at 0.1 V/s was also included (dashed curve). Inset shows the pH dependence of the formal potentials of peaks I and II.

potentials than what we observed here (Figure 5).[54] A more plausible explanation may be that the voltammetric profiles are actually due to charge transfer of peripheral functional moieties that are analogous to phenanthrenequinone derivatives. It is well-known that in aqueous media, phenanthrenequinone undergoes two-proton, two-electron redox reactions, leading to a cathodic shift of 59 mV with the increase of one pH unit at room temperature. The smaller shift as observed above with peak II (37 mV) suggests that approximately only one proton is involved in the faradaic process. Such a behavior has also been observed earlier with 9,10-phenanthrenequinone and ascribed to the adsorption of the reduced form onto the electrode surface by a phenolate moiety.[55] In fact, from Figure 5, one can see that the anodic wave of peak II indeed exhibits a surface waveshape. Furthermore, the existence of phenanthrenequinone derivatives on the carbon nanoparticle surface might also account for the observed merging of the two anodic waves of peaks I and II at decreasing potential sweep rate, as phenanthrenequinone and derivatives are known to decompose during electrochemical reduction.[56] Certainly, to have an unambiguous understanding of the molecular mechanism, further work is needed to unravel the structural details of the carbon nanoparticles.

Metal−Carbon Nanocomposites. The carbon nanoparticles obtained above may then be used to prepare carbon−metal nanocomposites. As mentioned earlier, experimentally, metal salts were reduced into nanostructured materials by ascorbic acid in the presence of carbon nanoparticles. The metal ions most likely bound to the peripheral carboxylic moieties by ion exchange or coordination reactions. Upon the addition of a reducing

(52) Kruis, F. E.; Fissan, H.; Peled, A. *J. Aerosol Sci.* **1998**, *29*, 511–535.
(53) Hanif, M.; Lu, P.; Li, M.; Zheng, Y.; Xie, Z. Q.; Ma, Y. G.; Li, D.; Li, J. H. *Polym. Int.* **2007**, *56*, 1507–1513.
(54) Lide, D. R. CRC Handbook of Chemistry and Physics: A Ready-Reference Book of Chemical and Physical Data, 85th ed.; CRC Press: Boca Raton, FL, 2004.
(55) Ishioka, T.; Uchida, T.; Teramae, N. *Anal. Chim. Acta* **2001**, *449*, 253–260.
(56) Soriaga, M. P. *Chem. Rev.* **1990**, *90*, 771–793.

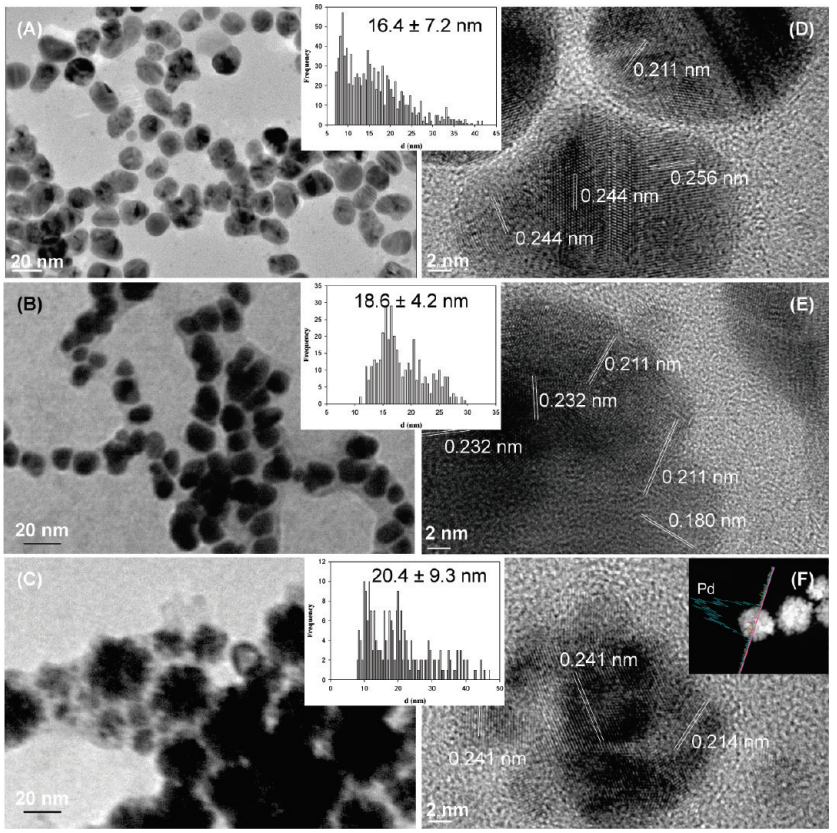

Figure 6. Representative TEM micrographs of carbon nanoparticles functionalized with different metal nanostructures: panels (A) and (D), silver; panels (B) and (E), copper; and panels (C) and (F), palladium. The crystalline lattices were identified in the respective HRTEM images. The central insets are the corresponding histograms of the overall particle size distribution. The upper-right inset to panel (F) depicts the elemental mapping of a palladium nanoparticle. Scale bars are 20 nm in the left panels, and 2 nm in the right ones.

reagent, the metal ions were reduced to metal atoms, which served as the nucleation seeds for the growth of metal nanostructures.[57] Figure 6 (panels A to C) shows the representative TEM micrographs of the nanocomposites loaded with three different metal nanostructures, (A) Ag, (B) Cu, and (C) Pd. It can be seen that the nanostructured particles are generally spherical in shape and the effective size is all much larger than that of the carbon particles (Figure 1). As depicted in the figure insets, the average size of the metal−carbon nanocomposites is 16.4 ± 7.2 nm (Ag), 18.6 ± 4.2 nm (Cu), and 20.4 ± 9.3 nm (Pd), respectively. Consistent results were also obtained in AFM measurements (not shown).

Whereas ascorbic acid is a relatively weak reducing agent, the reduction of metal ions and the generation of metal particles may be facilitated by the complex formation between metal ions and carbon nanoparticles through the peripheral carboxylic moieties. As the resulting composites are soluble in water (after extensive dialysis), it is very likely that the metal particles are surrounded by the carbon nanoparticles whose peripheral charges help stabilize the metal particles in solution. In fact, from low-resolution TEM imaging, a low-contrast halo ring (arising from carbon nanoparticles) can be seen wrapping around the high-contrast metal nanostructures (e.g., panels B and C), and in some cases, the metal particles appear to form chain-like structures embedded within a carbon matrix (panels B and C), suggesting that the deposition of the metal nanoparticles was initiated from the carbon particle surface.

Such a structural distribution is further confirmed by HRTEM measurements, as shown in panels D, E, and F, where the lattice fringes of the respective metals can be clearly defined (note that because of the much lower electron density, the lattice fringes of the carbon nanoparticles became difficult to resolve). For instance, in panel D, the lattice fringes of 0.244 and 0.211 nm may be ascribed to Ag(111) and Ag(200), respectively (JCPDS 4-0783). The distribution of silver over the composite nanostructures was further confirmed by elemental mapping (Supporting Information, Figure S4). In panel E, the Cu(111) and Cu(200) lattice planes can be identified with a fringe spacing of 0.211 and 0.180 nm, respectively (JCPDS 4-0836). In panel F, the HRTEM images show that the resulting Pd nanoparticles are highly crystalline, where a well-defined crystal lattice of 0.246 nm may be attributed to Pd(111). Furthermore, a closer examination indicates that the nanocomposites appear to be an aggregate of multiple small Pd particles. This is likely a result of the strong chelating interactions between Pd^{2+} and carboxylic functional groups which limit the growth of the Pd nanoparticles and concurrently cross-link the Pd particles, in agreement with the growth

(57) Yu, R. Q.; Chen, L. W.; Liu, Q. P.; Lin, J. Y.; Tan, K. L.; Ng, S. C.; Chan, H. S. O.; Xu, G. Q.; Hor, T. S. A. *Chem. Mater.* **1998**, *10*, 718–722.

dynamics of colloidal nanoparticles.[58] In fact, the "raspberry" features may be better illustrated in elemental mapping which clearly depicts the clustering of small Pd particles (inset to panel F).

The intimate interactions between the metal and carbon particles were also manifested in FTIR measurements. As shown in Figure 4, in comparison to the spectrum of the original carbon nanoparticles (black curve), there are at least three aspects that warrant attention. First, the ring C=C vibrational stretch at 1612 cm^{-1} remains practically unchanged. Second, the peak for carbonyl (C=O) vibration becomes much better-defined and shifts to 1723 cm^{-1}, in particular with C−Cu and C−Pd nanocomposites, whereas it remains very small with C−Ag particles. This may be explained by the different bonding interactions between the carboxylate groups and the transition metals (presumably through a thin metal oxide film formed on the metal surface), as it has been known that the two oxygen atoms of the carboxylate group would bind to the AgO_x surface nearly symmetrically whereas on CuO_x (and likely on PdO_x as well), the carboxylate binds asymmetrically with the tilting angle close to zero.[59] Such a structural discrepancy may also account for the drastic diminishment of the symmetric carboxylate vibrational bands at 1384 cm^{-1} and its split into two bands at 1340 and 1417 cm^{-1}. Third, the acid bending band at 1045 cm^{-1} becomes increasingly pronounced, which might be ascribed to the bonding interactions between the carboxylate moieties and the metal surfaces.

The C−Cu and C−Pd nanocomposites both exhibit a featureless UV−visible absorption profile that is consistent with Mie scattering (Supporting Information, Figure S2), whereas for the C−Ag particles a broadband emerges between 350 and 700 nm (peak at 380 nm), most probably as a consequence of the strong surface plasmon resonance of Ag nanoparticles. Interestingly, despite the well-known quenching effect of transition metals, the metal−carbon nanocomposites still exhibit well-defined photoluminescence responses, as depicted in Figure 4. Of note is that the excitation and emission peak energies appear to be virtually invariant among the three metal−carbon nanostructures, but with a red-shift of 20 to 35 nm in comparison to those of the original carbon nanoparticles (Figure 4). As the photoluminescence arose exclusively from the carbon nanoparticles, this observation implies that the emission was indeed determined by nanoparticle surface states that might be sensitively manipulated by the interactions with deposited metal nanoparticles. By taking into account the optical density at the corresponding excitation wavelength position, the effective quantum yield can be estimated to be about 36.7% (C−Ag), 33.4% (C−Pd), and 60.1% (C−Cu) of that of the carbon nanoparticles (it should be noted that the optical absorbance is a combined contribution of the carbon and metal nanoparticles, and only the carbon nanoparticles are fluorescent, thus the actual quantum yield should be higher).

(58) Chen, S. W.; Templeton, A. C.; Murray, R. W. *Langmuir* **2000**, *16*, 3543–3548.
(59) Ulman, A. *Chem. Rev*. **1996**, *96*, 1533–1554.

Conclusion

Carbon nanoparticles were prepared by acid treatment of combustion soot from natural gas. HRTEM and ^{13}C NMR spectroscopic measurements suggested that the particles were of graphitic structures with peripheral carboxylic acid/carbonyl moieties. Like their smaller counterparts, these particles exhibited well-defined photoluminescence properties, suggesting that the particles behaved as indirect bandgap materials and the photoluminescence arose from electronic transitions involving surface trap states. Furthermore, electrochemical measurements suggested that the carbon nanoparticle surface was functionalized with moieties that were analogous to phenanthrenequinone derivatives. Interestingly, the carbon nanoparticles might serve as unique structural scaffolds for the deposition of nanostructures of varied transition metals, leading to the formation of functional nanocomposites which remained highly luminescent.

Acknowledgment. The authors thank Prof. Q. Huo and Dr. J. Zou (UCF) for carrying out the XPS study. This work was supported in part by the National Science Foundation (DMR−0804049). L.T. thanks the China Scholarship Council for a research fellowship. TEM work was carried out at the Molecular Foundry and National Center for Electron Microscopy in Lawrence Berkeley National Laboratory which is supported by the U.S. Department of Energy.

Supporting Information Available: Additional HRTEM images, XPS and UV−visible spectra, and elemental mapping of carbon-transition metal nanocomposite particles. This material is available free of charge via the Internet at http://pubs.acs.org.